Integrated sedimentological and seismic reservoir characterization studies as inputs into a Lower Cretaceous reservoir geomodel, offshore Abu Dhabi

Ferran Pacheco[1*], Michael Harrison[2], Shraddha Chatterjee[2], Kiyotaka Ishinaga[1], Shunsuke Ishii[1], William Mills[2], Nathaly Vargas[2], Subhrankar Paul[2] and Pierre Roy[2] present a case study for building a 3D geological model to characterize a Lower Cretaceous reservoir for a field located offshore Abu Dhabi.

Introduction

Reservoir characterization plays a fundamental part in the development and/or appraisal of any hydrocarbon field. Understanding and quantifying the characteristics and distribution of the reservoir rock properties is an evaluation step that needs to be performed before starting any reservoir model. An accurate description of the reservoir is vital to help appropriately manage and optimize oil recovery. From core to seismic scale, any relevant piece of information should be integrated in order to reduce uncertainties, and optimize understanding of the final flow behaviour and fluid distribution inside the reservoir. The goal of the final geomodel is to obtain consistent properties that are driven by the geological facies models (including depositional facies and diagenesis; reservoir rock types) and trended by the seismic information.

This paper presents a detailed and integrated methodology and case study for building a 3D geological model to characterize a Lower Cretaceous reservoir for a field located offshore Abu Dhabi. During this study, data sets from two cored and seven uncored wells were utilized for sedimentological interpretations and sequence stratigraphic analysis to establish a consistent high-resolution sequence stratigraphic framework. The detailed descriptions were linked to the petrophysical properties derived from the conventional core analysis (CCAL) and mercury injection capillary pressure (MICP), developing a new reservoir rock type classification (RRT). Several hydraulic flow units (HFU) were identified and used to evaluate which intervals are the major flow contributors. The identification of these HFUs offers a link between the fluid flow, geological framework and RRTs. From achieving a deep understanding of the facies associations (FA) and the reservoir properties in core, these interpretations have been extrapolated into the uncored wells based on specific log responses and the developed geological conceptual model. Several depositional environment maps were generated for each high-resolution stratigraphic sequence and were used as a guideline for the facies modelling. The objective of the modelling grid is to reproduce the depositional and diagenetic model including the petrophysical behaviour captured by the integrated rock type classification. Good-quality 3D seismic data was used to enhance the characterization of the reservoir in the interwell areas by improving the spatial prediction of petrophysical properties achieved during the seismic inversion. Seismically derived 3D porosity realizations were generated using a geostatistical approach and then used as a secondary variable to guide porosity distribution on the final 3D geological model.

General information

The work was carried out on a new light oil field development, with less than one year of production history, located offshore Abu Dhabi (Figure 1). The development included both vertical

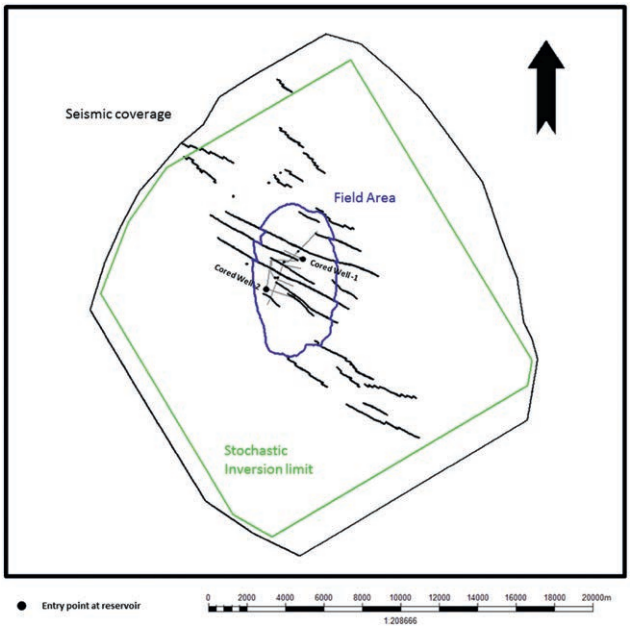

Figure 1 Field map with seismic coverage, stochastic inversion limit and the location of the ten uncored wells and two cored wells.

[1] ADOC | [2] CGG
* Corresponding author, E-mail: ferran@adoc.ae
DOI: 10.3997/1365-2397.2019027

appraisal wells and horizontal producers, and this case study was performed during the drilling development campaign.

A good set of data was available to build the geological framework and seismic inversion:

- 3D seismic data were acquired in 2014 and processed in 2014-2015 covering an extensive area.
- 12 wells were available:
  - seven vertical/low deviation wells (2 cored) located at the crest
  - two horizontal wells at the crest (used as blind test wells)
  - three vertical wells located at the flanks
- A good set of logs with complete petrophysical interpretation
- 325 ft of core including good coverage of thin sections, CCAL and MICP

Structure and reservoir characteristics

The field is a south-north oriented anticline with four-way dip closure (Figure 1). Faults are clearly seen on the 3D seismic data, with dominant normal fault components and a strike-slip component. The reservoir thickness is around 150 ft and is described as an eastward prograding shallow-marine carbonate platform/shelf. There is significant vertical degradation of the reservoir properties towards the bottom of the reservoir with subtle lateral changes in the porosity observed from well to well.

Geological background

The interval of interest to this study is of Valanginian to Aptian age (Strohmenger et al., 2006). During the Early Cretaceous period, Abu Dhabi was part of a broad shallow marine platform with no significant land mass developed in the proximity of the study area. The sediments are therefore dominated by shallow marine carbonate platform facies typical of the Early Cretaceous Neo-Tethys (e.g. Ziegler, 2001; van Buchem, 2002). With the development of the Bab Basin to the north during the Aptian period, the succession represents a relatively deeper section compared to the shallow marine carbonates of the Valanginian.

Facies and sequence stratigraphy

On the basis of data obtained from the detailed core descriptions 22 facies and six FAs were identified. Through the main reservoir section, the vertical succession passes through three broad platform types (Figure 2):

1. Rudist-dominated platform
2. Lithocodium-Bacinella-dominated platform
3. Orbitolinid, micrite-dominated platform

The main reservoir section represents a shallowing-upward trend from an open marine middle ramp environment consisting of mostly skeletal, peloidal and orbitolinid packstones and wackestones. Water depths are probably only in the low tens of metres, and wave energy is relatively low. Lithocodium-Bacinella skeletal packstones, floatstones and boundstones have a patchy distribution within the upper ramp setting, with the boundstones probably providing stabilization of the substrate for subsequent rudist and shoal development, and also providing the sediment for the associated locally reworked packstone/floatstone facies.

As deposition becomes shallower towards more proximal settings the Lithocodium-Bacinella deposits consist of packstones and floatstones. They predominantly comprise rip-up clasts of Lithocodium-Bacinella debris. The floatstones generally appear to be slightly higher-energy deposits than the packstones, often forming small-scale coarsening-upwards cycles.

The Lithocodium-Bacinella deposits are interpreted to form the antecedent topography that the rudists colonize. The rudist shoal/build-ups are dominated by rudist, peloidal floatstones with rare rudstones. In situ rudists are rarely seen; they are interpreted to be living and growing within the muddy, peloidal sediment as localized patches. The rudist facies are commonly interfingered with skeletal packstones and grainstones, along with skeletal/peloidal/coated-grain grainstones.

The rudists are capped by relatively thin (1-2 ft) skeletal/peloidal/coated-grain grainstone shoals. The grainstone intervals are typically bioturbated and locally planar to low-angle cross-laminated. They are interpreted as being the highest-energy facies, and probably indicative of shallow shoal development within the wave-affected zone. Locally, very thin layers of grainstone are present at the tops of parasequences, typically cemented during periods of exposure.

On a facies scale the well-to-well correlation was relatively consistent (well spacing at ~2 km). Sequence boundaries (SBs) and maximum flooding surfaces (MFSs) were identified within the two cored intervals and extrapolated into uncored sections and wells. The sequence stratigraphic interpretation has been reviewed and adapted from Strohmenger et al. (2006). The main reservoir section represents a highstand system tract with a major sequence boundary at the top.

Based on the mapped higher-scale sequences and associated facies deposited, key surfaces that bound major vertical changes in porosity in the reservoirs were identified. Reservoir quality is broadly controlled by stacked facies relationships. However, post-depositional diagenetic controls have also had an impact.

Facies maps and detailed sedimentological descriptions were used to generate a comprehensive and simplified facies framework of the reservoir (Figure 3). This framework was used to build the skeletal framework to run a stochastic seismic inversion and to constrain the distribution of petrophysical properties in the 3D geological model.

Well Reservoir Characterization (Core/Log)

Rock typing workflow

The RRT classification is used to discriminate an interval of rock with consistent and predictable geological and petrophysical properties that will affect the fluid distribution and flow. This classification aims to highlight the link between the geological descriptions from the core (geological rock types (GRT)), which are based on textural features of the original fabric and the diagenetic processes, and the petrophysical properties derived from the CCAL and MICP (petrophysical rock types (PRT)) (Figure 4). Each rock type (RT) is deposited under a similar environment (i.e. number of the RT code) and has undergone similar diagenetic alterations (i.e. letter of the RT code). A unique porosity/permeability relationship (with minimal overlap between each

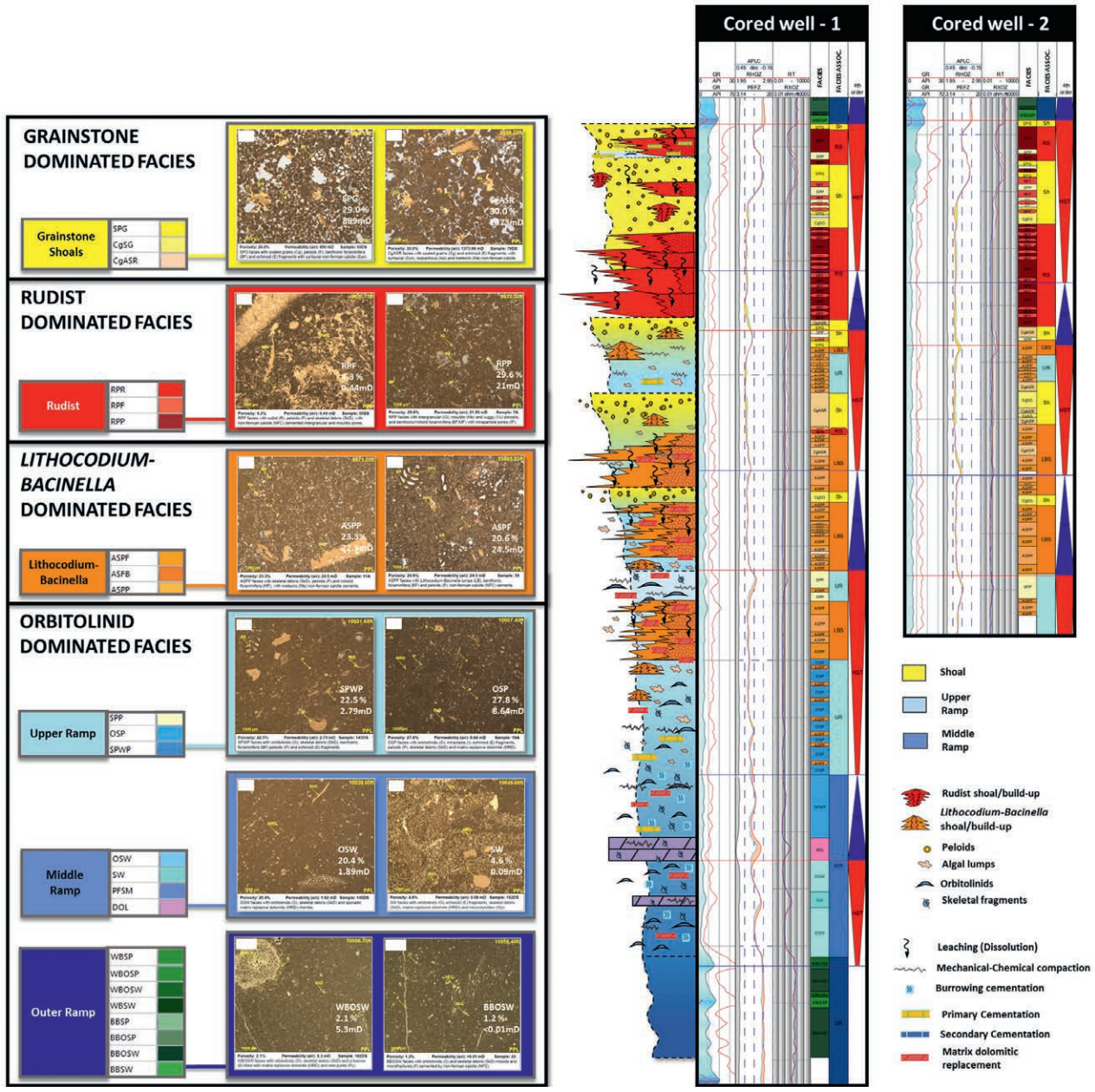

Figure 2 Right: Vertical profile of the two cored wells with schematic core description. Left: The six FAs and their constituent facies with representative photomicrographs.

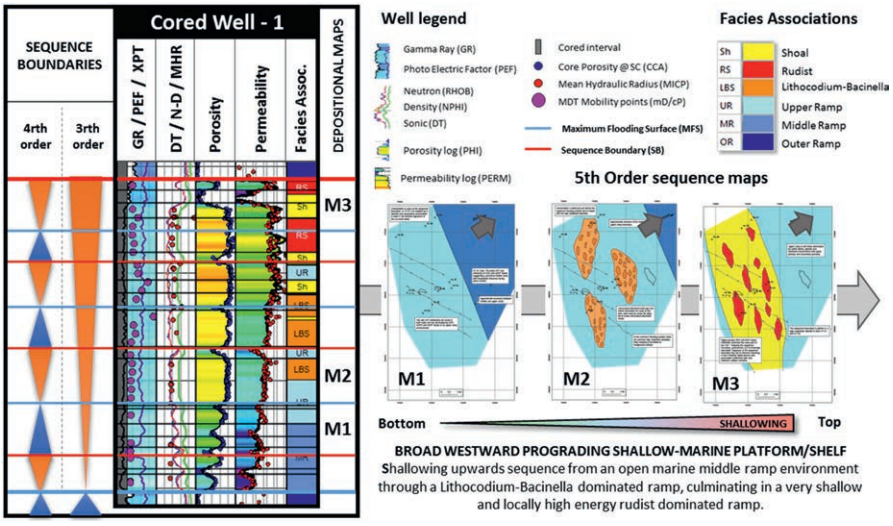

Figure 3 Summary of the sedimentological study showing the newly developed sequence stratigraphic framework and depositional maps with the different FAs. Cored well-1 is shown as reference for the log response.

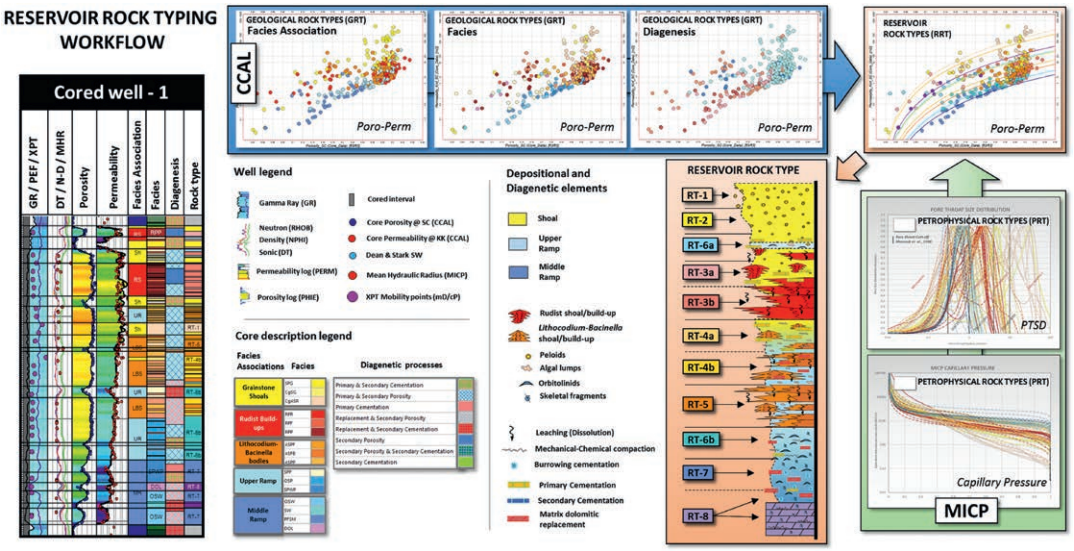

Figure 4 Summary of the workflow used to generate the different RRTs.

FACIES ASSOCIATIONS	RESERVOIR ROCK TYPES (RRT)	GEOLOGICAL ROCK TYPES (GRT) — Predominant Facies and Diagenetic processes (Core & thin section description)	PETROPHYSICAL ROCK TYPES (PRT) — Porosity-Permeability (CCAL)	Pore throat Size Distribution (MICP)	Capillary pressure (MICP)
Shoal skeletal /peloidal /coated-grain grainstones	**ROCK TYPE 1**	• Dominated by Coated-grain, algal, skeletal rudstone/floatstone (CgASR) • Preservation of primary intergranular and intraparticle porosity			
	ROCK TYPE 2	• Coated-grain, skeletal peloidal grainstone (CgSGS – SPG) • Preservation of primary intergranular and intraparticle porosity. Initial cementation of primary intergranular and intraparticle porosity			
Rudist shoal/build-up	**ROCK TYPE 3A**	• Rudist, peloidal packstone and floatstone (RPP-RPF) • Initial cementation of primary intergranular and intraparticle porosity, and secondary mouldic porosity by leaching	A	N/A	N/A
	ROCK TYPE 3B	• Rudist, peloidal packstone and floatstone (RPP-RPF) • Preservation of primary intraparticle and intergranular porosity and Increased vuggy porosity as a result of dissolution enhancement of rudist mouldic porosity	B		
Lithocodium-Bacinella shoal/build-up	**ROCK TYPE 4A**	• Algal, skeletal, peloidal floatstone/rudstone (ASPF) • Affected by Mechanical and chemical compaction and reduction of intergranular porosity due to primary pore cementation	A	N/A	N/A
	ROCK TYPE 4B	• Algal, skeletal, peloidal floatstone/rudstone (ASPF) • Common to abundant matrix replacement by sub-planar dolomite. Vuggy enhancement of Lithocodium-Bacinella intraparticle porosity	B		
	ROCK TYPE 5	• Algal, skeletal packstone (ASPP) • Open intraparticle porosity of Lithocodium-Bacinella is enhanced by local dissolution producing vuggy pores. Partially cemented primary intergranular porosity preserved pore space from compaction			
Upper Ramp orbitolinid packstone	**ROCK TYPE 6A**	• Skeletal, peloidal orbitolinid packstone (SPP-OSP) • Primary intraparticle, secondary mouldic and vuggy porosity is partially cemented	A	N/A	N/A
	ROCK TYPE 6B	• Skeletal, peloidal orbitolinid packstone (SPP-OSP) • Decreased porosity due to chemical compaction associated cementation of skeletal moulds. Additional to dolomite replaced and mechanically compressed matrix.	B		
Middle Ramp orbitolinid packstone /wackestone	**ROCK TYPE 7**	• Skeletal, peloidal, orbitolinid wackestone/packstone (SPWP-OSW) • Matrix replacive dolomite is common in burrowed facies. Partial cementation of primary intraparticle and secondary mouldic pores			
	ROCK TYPE 8	• Skeletal wackestone + Dolomite (Middle ramp) (DOL – SW) • Increased pressure solution and matrix replacement by dolomite. Leaching and cementation of skeletal grains. Saddle dolomite occludes larger secondary pores		N/A	N/A

Figure 5 Summary table of the RT classification illustrating the correlation between the geological description from the core and the petrophysical properties derived from the CCAL and MICP data.

RT), capillary pressure profile and pore throat size distribution also imprint each RT.

The skeletal/peloidal shoal-dominated, rudist-dominated, Lithocodium-Bacinella-dominated and orbitolinid mud-dominated FAs have each their own individual reservoir characteristics and it is on this basis that they were separated. The RRT classification integrates sedimentological, diagenetic and petrophysical properties (Figure 5).

Reservoir quality

The best reservoir properties are found in the high-energy skeletal/peloidal grainstone and rudstone shoal facies (RRT-1 and RRT-2). Early marine cementation has preserved intergranular porosity and this has resulted in a well-connected pore network with very high permeability values. These high porosity and permeability intervals have been observed in both cored wells and are correlatable through the entire field.

Generally, the rudist facies also present good reservoir-quality properties (RRT-3A and RRT-3B). They are dominated by packstones and floatstones with rudist fragments. These facies have been affected by leaching, which resulted in large secondary mouldic and vuggy pores that are well connected by intergranular pores and microporosity.

Lithocodium-Bacinella facies have moderate-to-good reservoir properties (RRT-4A, RRT-4B and RRT-5). These are related to algal and skeletal packstones and floatstones. These facies are dominated by intraparticle porosity with localized enhanced reservoir properties and permeability through dissolution processes (e.g. RRT-5). Localised cementation, increased compaction and stylolites have reduced both primary and secondary porosity and decreased the permeability (e.g. RRT-4A).

The open marine upper/middle ramp environment is dominated by skeletal, peloidal and orbitolinid packstones and wackestones (RRT-6A, RRT-6B, RRT-7). Primary intraparticle, secondary mouldic and vuggy porosities tend to be partially cemented while the matrix is mechanically compressed. Microporosity is important due to the micritic composition of the sediments. A continuous layer of dolomite is observed along the field (RRT-8); it is composed of dolomitised skeletal wackestones. Overall, this interval has the poorest reservoir properties.

Various attempts at using 'artificial neural networks' based on the logs were used to predict the core-based RTs at the log scale in the uncored wells and intervals (supervised classification). Unfortunately, many input logs are not sensitive to the main characteristics of the RTs, and more importantly, they are not able to capture the permeability changes that have been defined by the classification. Therefore, a more deterministic approach, based on the conceptual geological model (depositional and diagenetic), the available pore size partitioning logs (CMR) and some dynamic information, was used to extrapolate the RT classification into the uncored wells and intervals. An independent porosity-permeability regression function for each RT was used to reproduce a permeability curve. By applying this algebraic permeability transform to the porosity log, in all the wells, the permeability was then upscaled and used as an input into the geological model (Figure 6).

The ultimate quality check (QC) was to compare the water saturation based on a saturation height function (core-derived

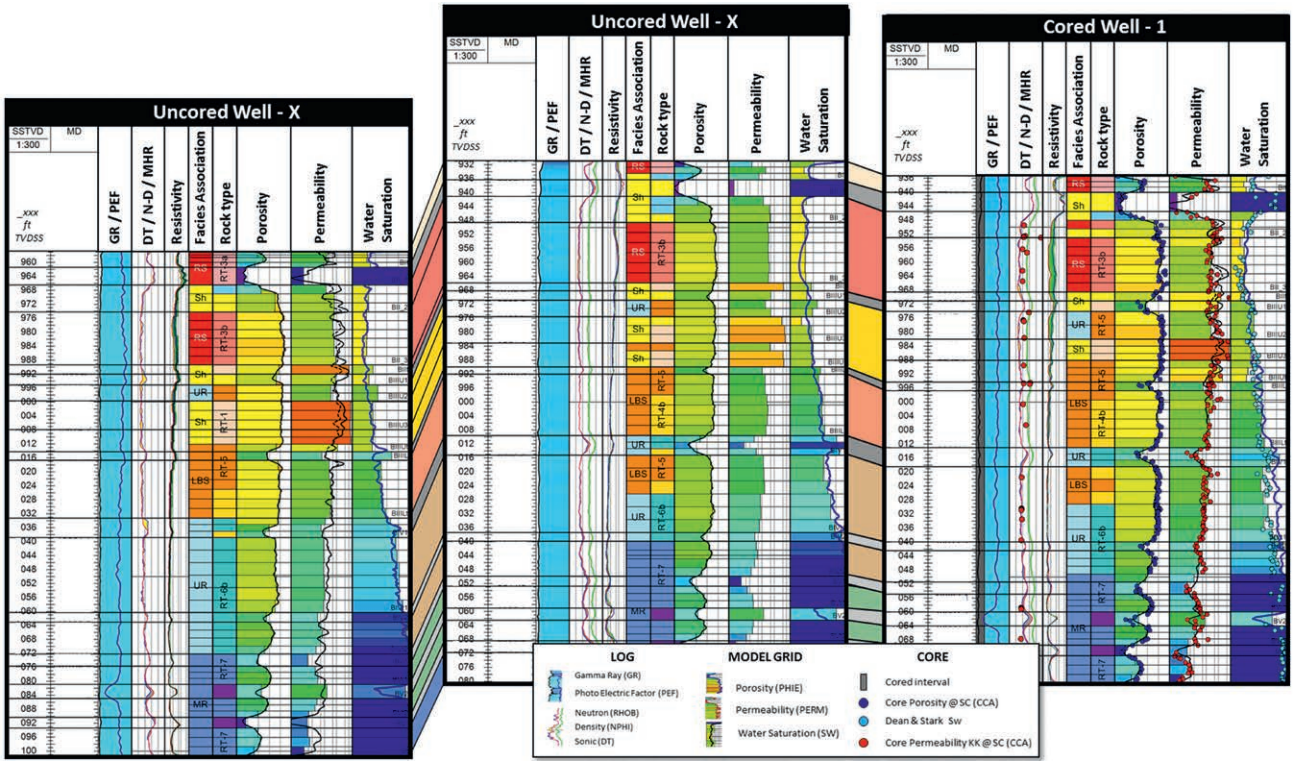

Figure 6 Correlation between Cored Well-1 and two uncored wells, illustrating the predicted permeability log (upscaled) and the final water saturation based on a Saturation Height Function (core-derived J-Function per RT (SwSHF)). The good match between Water Saturation from the resistivity log (SwLog) (black line) and the SwSHF (model cells) supports the current distribution of the RTs in the uncored wells.

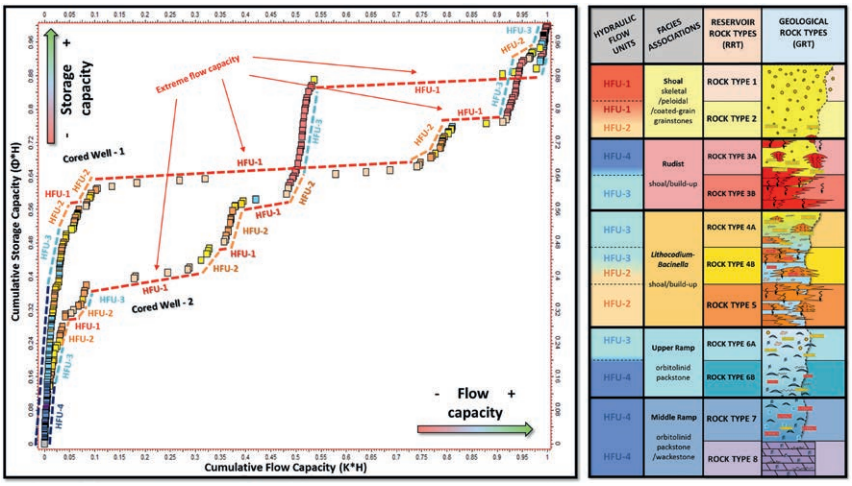

Figure 7 Left: SMLP illustrating the percentage flow capacity (permeability*height) versus percentage storage capacity (porosity*height) ordered in stratigraphic sequence. Right: Table comparing the identified HFUs and RRT classification.

J-function per RT (SwSHF)) and the water saturation based on the resistivity logs (SwLog). A good match between both saturations may indicate a good link to the predicted RT (Figure 6).

Hydraulic flow units (HFU)

A stratigraphic modified Lorenz plot (SMLP) was used to evaluate which intervals are the major contributors to the flow. The graph illustrates the percentage flow capacity (Permeability*Height) versus percentage storage capacity (Porosity*Height) ordered in stratigraphic sequence (Figure 7). A continuous sampling rate is generally required in order to obtain a representative flow distribution. The CCAL sampling rate of the cored wells is continuous (every foot), which made them very good candidates for this exercise as it offers a guide to see if the flow units honour the geologic framework and the RRTs. The key flow unit characteristics identified are partial barriers (seal to flow; HFU-4), speed zones (conduits; HFU-1), and baffles (zones that throttle fluid movement; HFU-2 and HFU-3). Intervals with similar slopes will correspond to the same HFU. A set of vertical cumulative curves were generated by using the same percentage Porosity*Height and percentage Permeability*Height to help better identify the contributors to the flow and identify the lateral continuity of each stratigraphic interval. The data was normalized from 0% to 100%, with 0% being null storage/flow capacity and 100% the maximum observed storage/flow capacity. Two curves of cumulative flow and cumulative storage were then generated from the bottom section of the reservoir and presented in a log track (Figure 8).

Four hydraulic flow units (HFU-1 to HFU-4) were identified in this reservoir interval. Flow capacity is very high in HFU-1, which is dominated by RRT-1 and RRT-2 composed of high-energy skeletal/peloidal grainstones and rudstones with well-connected primary intergranular pores (good permeabilities). These fluid conduits are in both cored wells, but in Cored Well-1, almost 60% of the flow contribution is concentrated within the same stratigraphic interval whereas in Cored Well-2 the flow is distributed across several intervals. The lateral continuity of this high-permeability conduit is observed along the field with a decrease in the flow capacity towards Cored Well-2 (Figure 8). HFU-2 is related to RRT-5 and occasionally RRT-4B. Flow capacity is significantly lower than HFU-1 and is similar to HFU-3. The facies related to these RTs are dominated by intraparticle porosity with local dissolution that has created secondary porosity. HFU-3 is identified in the layers where RRT-3B, RRT-4B and RRT-6A occur. Lithocodium-Bacinella intraparticle porosity and rudist mouldic porosity have been locally enhanced, although this has not significantly improved the permeability. This is shown by the higher storage capacity compared to the flow capacity. HFU-4 has good storage capacity but almost nil flow capacity. This is related to the occurrence of RRT-6B, RRT-7 and RRT-8, which are stratigraphically located at the bottom of the reservoir section (middle/outer ramp facies). The presence of microporosity related to the dominant micritic composition of the sediments provides good porosity values that are not connected. This is supported by the log saturations of the structurally higher wells of the field where almost no hydrocarbon was identified in the same stratigraphic interval (Figure 6). HFU-4 is also present in the upper part of the reservoir corresponding to the RRT-3A and occasional RRT-2. The upper part of the reservoir is affected by an early intergranular and intraparticle cementation that has negatively affected the reservoir properties of a depositionally good-quality facies.

There is a good correlation between the HFU and the RRT. The link between the GRTs and the petrophysical properties (PRT) leads to a better understanding of the fluid distribution within each well. The stratigraphic framework and the FA maps together with the lateral understanding of the flow units to allow for a more confident distribution of the RRTs into the inter-well areas through the 3D model.

Seismic reservoir characterization

Input data for stochastic seismic inversion

High-quality 3D seismic data was acquired in a logistically and operationally challenging field located at the near-shore covering shallow water (0 to 20 m) and an island area. Deployment of multiple types of seismic sources and dual-sensor receivers along the topographic surface, connected through cable, helped to overcome the otherwise complex logistical challenges. The variations, due to the use of different sources and receivers for the seismic data acquisition, were harmonized during the seismic data processing and imaging. Futhermore, well-driven velocity

model building and interpretation-guided seismic data processing produced reliable seismic data quality, resulting in the delivery of reliable inversion results.

A field-scale study always requires diagnostic multiple QCs of (a) multiple well logs of the area done through rock physics and (b) denoising of the seismic data in the

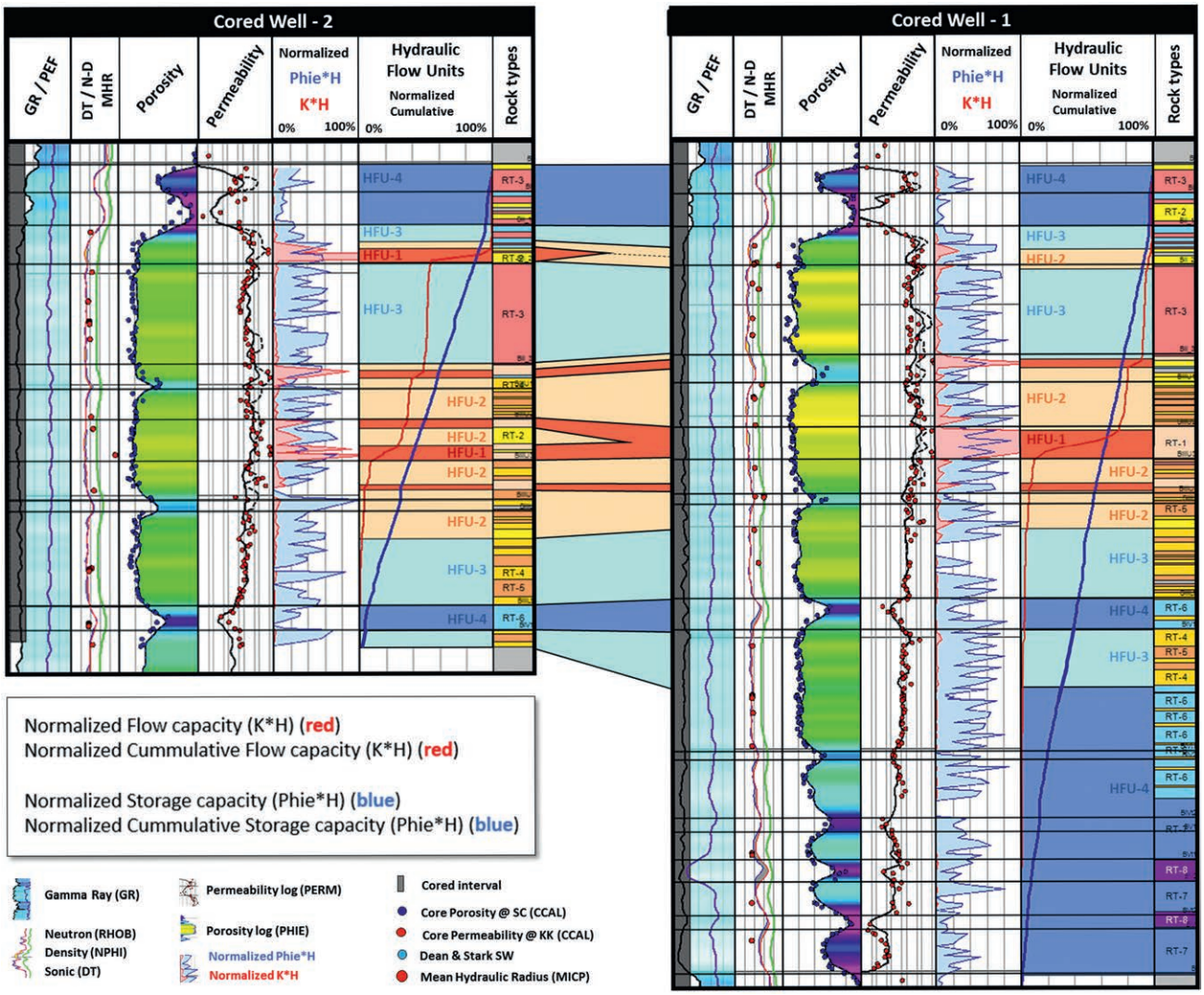

Figure 8 Correlation of the identified HFUs between the two cored wells.

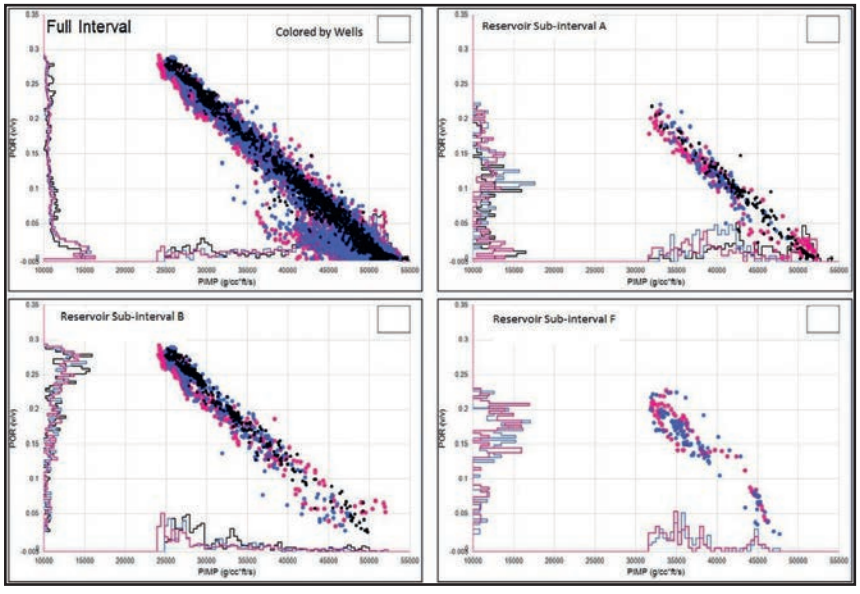

Figure 9 Rock physics crossplots of total porosity (Y-Axis) vs P-impedance (X-Axis) using modelled logs. Top left: Interval = full interval including all reservoirs of interest; Top right: Interval = sub-interval at reservoir unit A; Bottom left: Interval = sub-interval at reservoir unit B; Top right: Interval = sub-interval at reservoir unit F. All crossplots are coloured by wells.

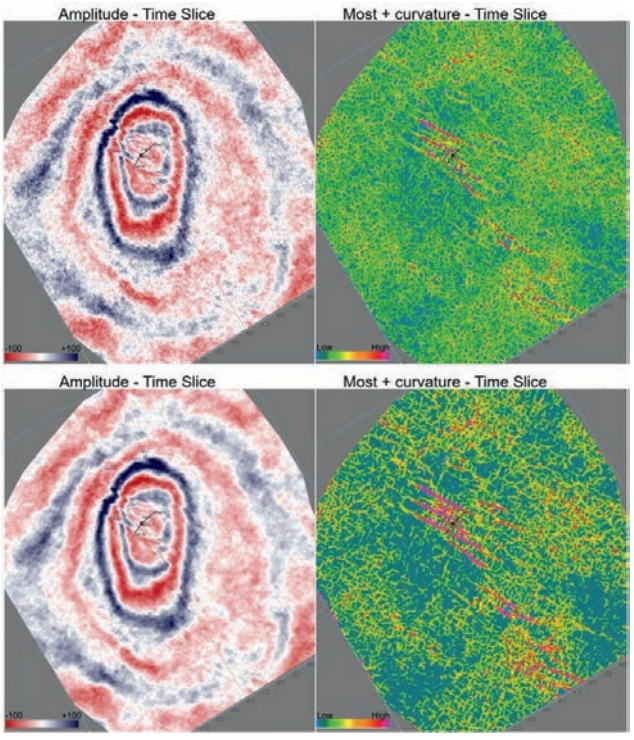

Figure 10 Time slice QC comparison of raw (top row) vs conditioned (bottom row) seismic amplitude (left-hand side) and its derived seismic attribute, most positive curvature (right-hand side).

post-stack domain during reservoir-oriented seismic data conditioning.

The objective of the rock physics modelling is to provide a link between the petrophysical properties and the elastic properties of the rocks (Vp, Vs, ρ). This link makes it possible to determine the elastic properties of the rocks through seismic inversion, which are interpreted in terms of reservoir properties. The model looked at three intervals, but the main interval of interest to this study was reservoir sub-interval B (discussed in this paper). The other intervals are illustrated here for comparison (Figure 9). Both empirical (multi-linear regression) and differential effective medium (DEM) approaches were analysed. DEM was found to be more suitable for modelling. This approach not only produced missing P- and S-logs but also validated the quality of newly derived petrophysical logs at newly-drilled well locations.

All seismic data, post-stack or pre-stack, contain noise. Typically, this noise is comprised of both coherent and random components (Dorn, 2018). Seismic data conditioning is a key improvement driver for any quantitative seismic interpretation or reservoir characterization project. Post-stack data conditioning for this data set comprised of a structurally oriented footprint removal process followed by application of an anisotropic diffusion filter. Most conventional methods of footprint removal use a planar, horizontal operator. Conventional methods of footprint removal using horizontal operators can potentially mix amplitude information from different reflections (Figure 10).

At least four de-striping steps were applied to the seismic data. The anisotropic diffusion filter is an iterative process that allows diffusion along the local orientation of seismic strata, while smoothing across smaller discontinuities. The anisotropic diffusion filter reduces the noise in the seismic volume by enhancing the edges of larger features such as horizons and faults.

Stochastic seismic inversion to porosity co-simulation

The seismic inversion process is inherently non-unique, which means that there are numerous elastic property models that fit the seismic data with equal probability (Trudeng et al., 2014). During stochastic inversion, this large model space constrained with geological information is sampled to identify gelogically consistent solutions. A stochastic seismic inversion algorithm uses a Bayesian framework (Buland et al., 2003) to determine the impedance probability density functions from seismic and well information. The following key steps were followed during the seismic inversion: (1) geological model building (2) well data upscaling (3) prior model building (4) variogram modelling. 150 equally probable, high-frequency models (Figure 11) of acoustic impedances with minimum layer thickness of 1ms (around 3.5 ft) were generated. Such fine-scaled layering ensures that results are closer to the geomodel scale.

Using the stochastic inversion impedances, 150 porosity realizations were generated through collocated sequential Gaussian simulation. The multiple porosity solutions made it possible to account for uncertainties that could be evaluated in a suite of numerical models to finally obtain a geomodel with good predictability.

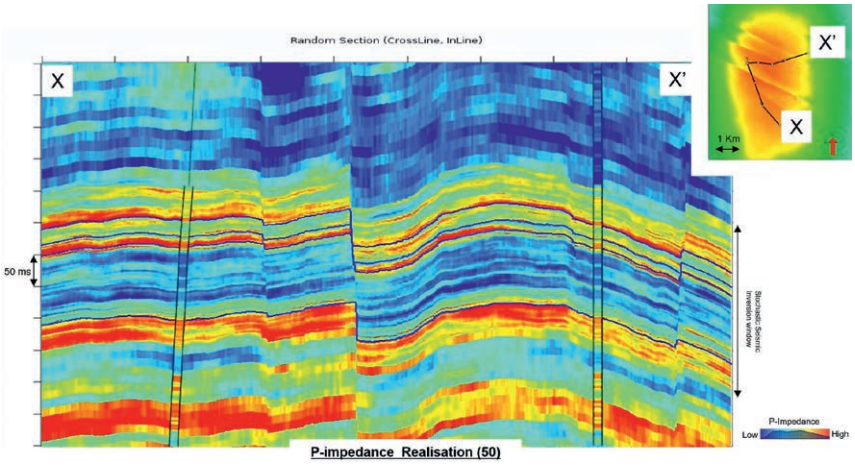

Figure 11 Random line section of Stochastic Inversion result (inverted P-impedance in m/s*g/cc) through the field passing from X' to X across major fault boundaries. The inverted P-impedance result is the P50th realization after ranking. The coloured columns on the section are well log P-impedance where P-impedance= P-velocity x density.

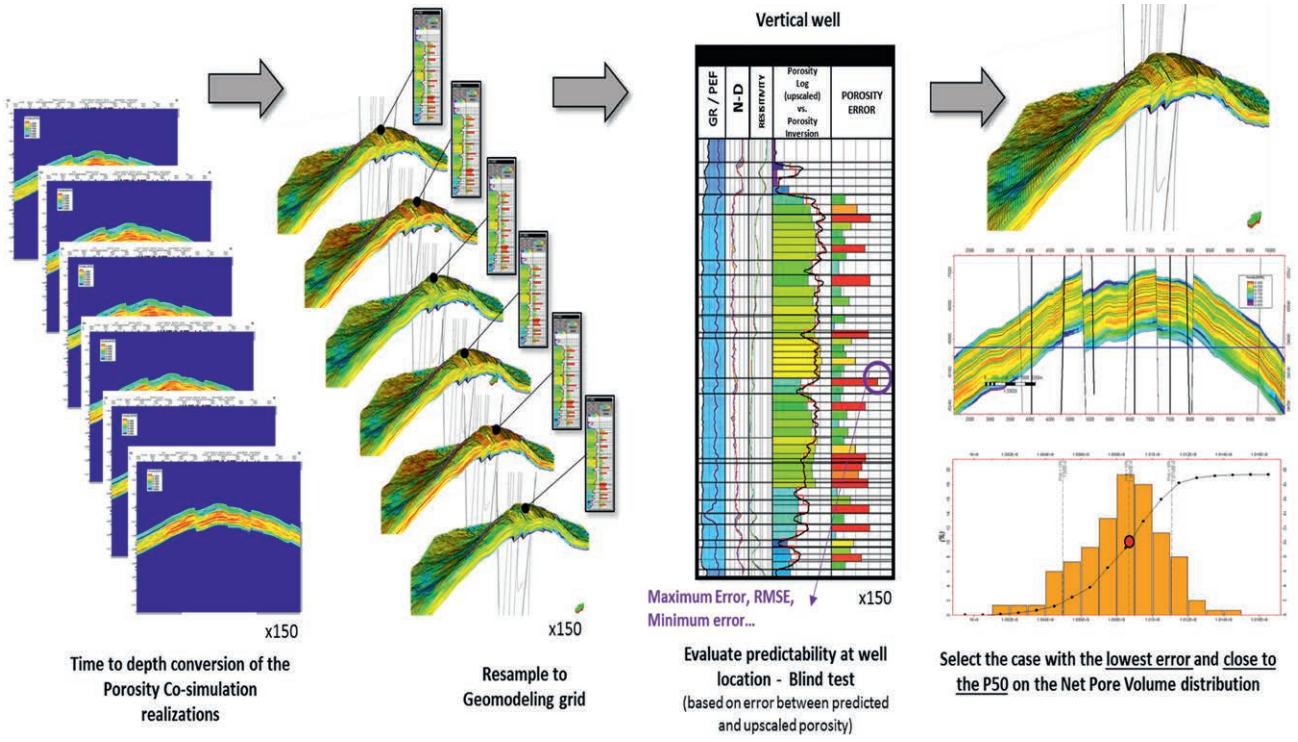

Figure 12 Summary of the workflow used to select the porosity co-simulation realization from the Stochastic Inversion (SI) that was used as an input on the geological model to distribute the final porosity.

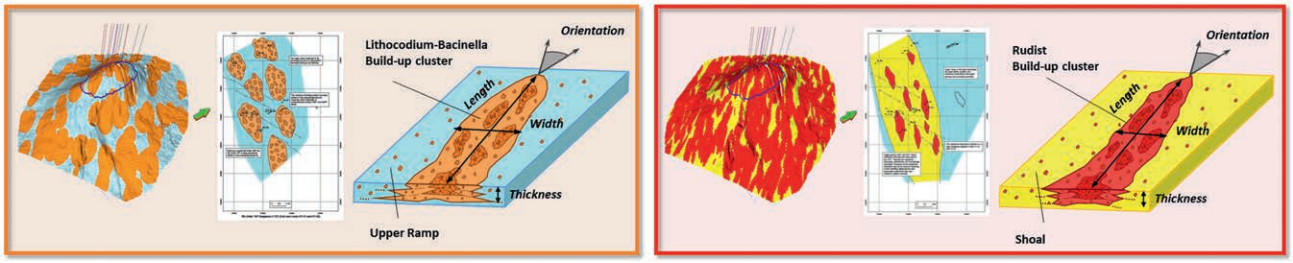

Figure 13 Geometrical inputs controlling the body shape (width, thickness, length, azimuth, etc.) of the FAs based on the sedimentological study.

Screening of stochastic seismic inversion results

Apart from the qualified wells used in the stochastic inversion, some other wells were chosen as blind wells where the porosity simulation results were validated. The 150 final porosity cubes were depth-converted and resampled to the 3D geological modelling grid. The porosity log was upscaled and the errors between the upscaled porosity log and the resampled porosity cubes were calculated on blind wells (at each cell). The net pore volume calculation was carried out above the free water level for all the porosity realizations. The selected realization used on the geological model for porosity distribution meets two conditions in this study: it has the lowest error in the porosity prediction at the blind wells and has a net pore volume close to the P50 (Figure 12).

Integration within the 3D geological model

Facies modelling

Facies modelling is performed in three main steps following a hierarchical method, where the gross depositional environment (GDE) constrains the distribution of the FAs and controls the RRT distribution. The objective is to reproduce the depositional model defined in the sedimentological study and include the petrophysical behaviour that is captured by the RT classification from the reservoir characterization study.

In the first step, the truncated Gaussian simulation algorithm was selected to model GDEs, taking into account natural transitions between sequences of facies. The lateral and vertical trends used for the 3D model honour the observations from the cored well and the predicted facies from the uncored intervals and wells. The reservoir is subdivided into three main environments organized into a shallowing upwards sequence from an open marine middle ramp environment through a Lithocodium-Bacinella dominated upper ramp, culminating in a very shallow and locally high-energy rudist-dominated ramp/shoal. The final product reproduces a broad eastward prograding shallow-marine platform (Figure 14).

In step two, the depositional elements corresponding to the FAs were populated within the previously modelled GDE. The object modelling algorithm was used to stochastically generate and distribute those architectural elements. The Lithocodium-Bacinella build-up clusters and the rudist build-up clusters were distributed using this method. All geometrical inputs controlling the body shape (width, thickness, length, azimuth,

etc.) were extracted from the sedimentological study. The FA maps were used as guidelines for the lateral distribution of those elements. Variability was given to the geometrical inputs controlling the geobody shape in order to assess the uncertainty related to their size and the orientation (Figure 13).

Finally, in the third step, the RRTs were populated and constrained by the FAs and the GDEs (Figure 14). These RRTs ultimately control the distribution of the reservoir properties within the model (porosity, permeability and water saturation). The sequential indicator algorithm is one of the most appropriate algorithms to use in reservoir modelling when the shape of a particular facies body is uncertain, in this case the RRT. This stochastic method required vertical and horizontal variograms as input.

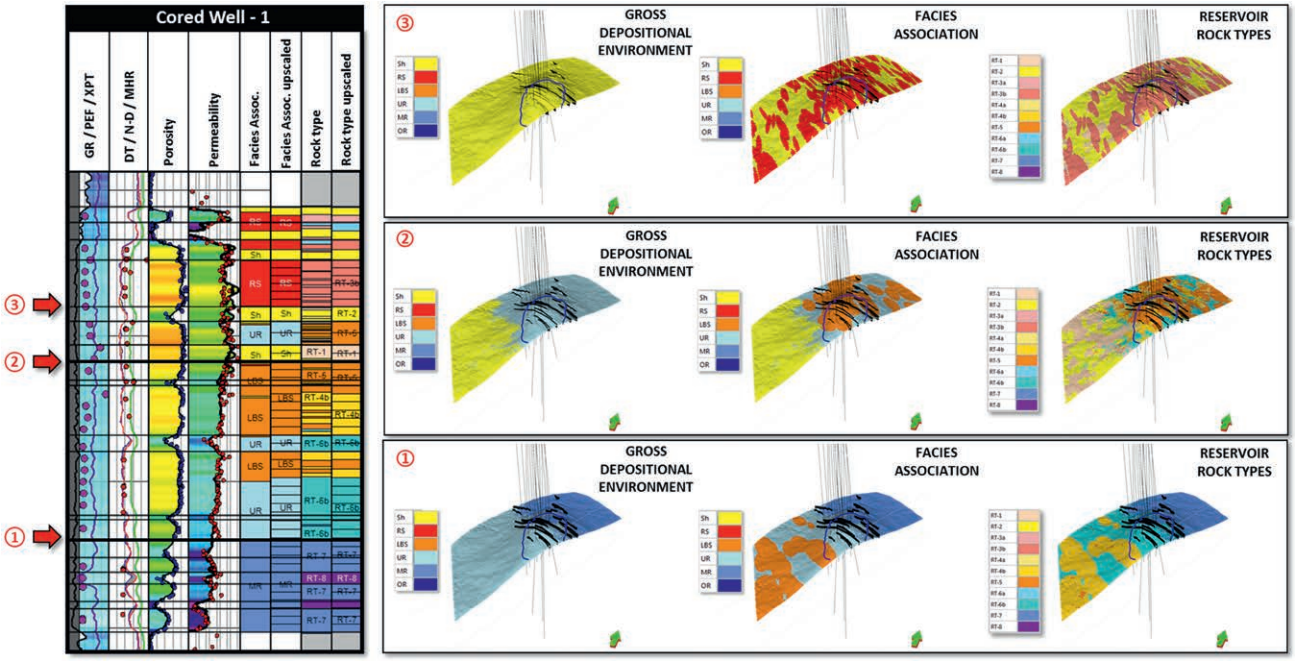

Figure 14 Example of three layers in the geological model illustrating the hierarchical character of the facies modelling process. Notice that the model reproduces the aspect of a broad westward prograding shallow-marine platform.

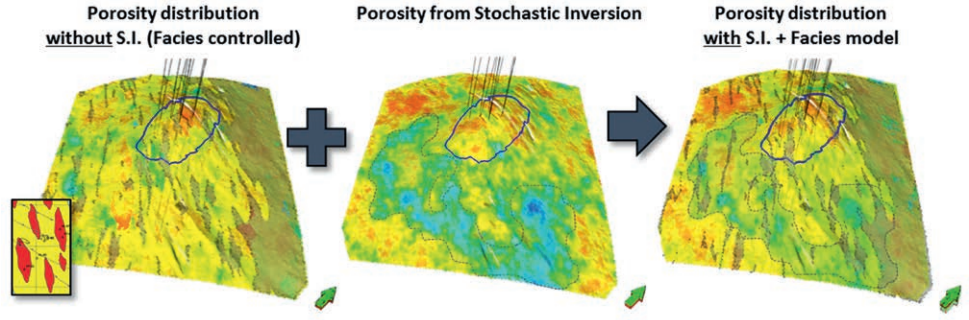

Figure 15 Illustration of one realization of the porosity model showing the impact of combining both the depositional model (RT distribution) and the results from the seismic inversion.

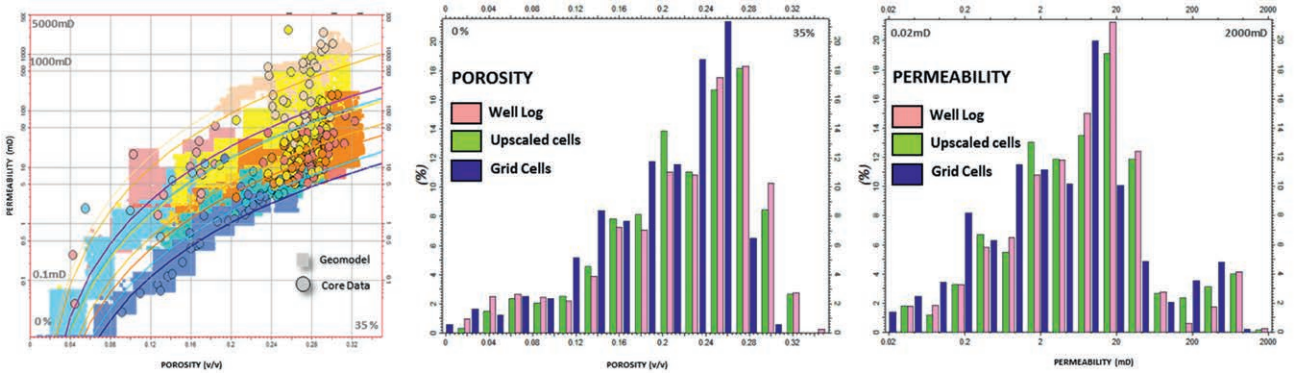

Figure 16 Set of graphs illustrating the QC between the input data (log, core and upscaled cells) and the results of the final model. Left: porosity-permeabiliy plot, Centre: porosity frequency histogram, Right: permeability frequency histogram.

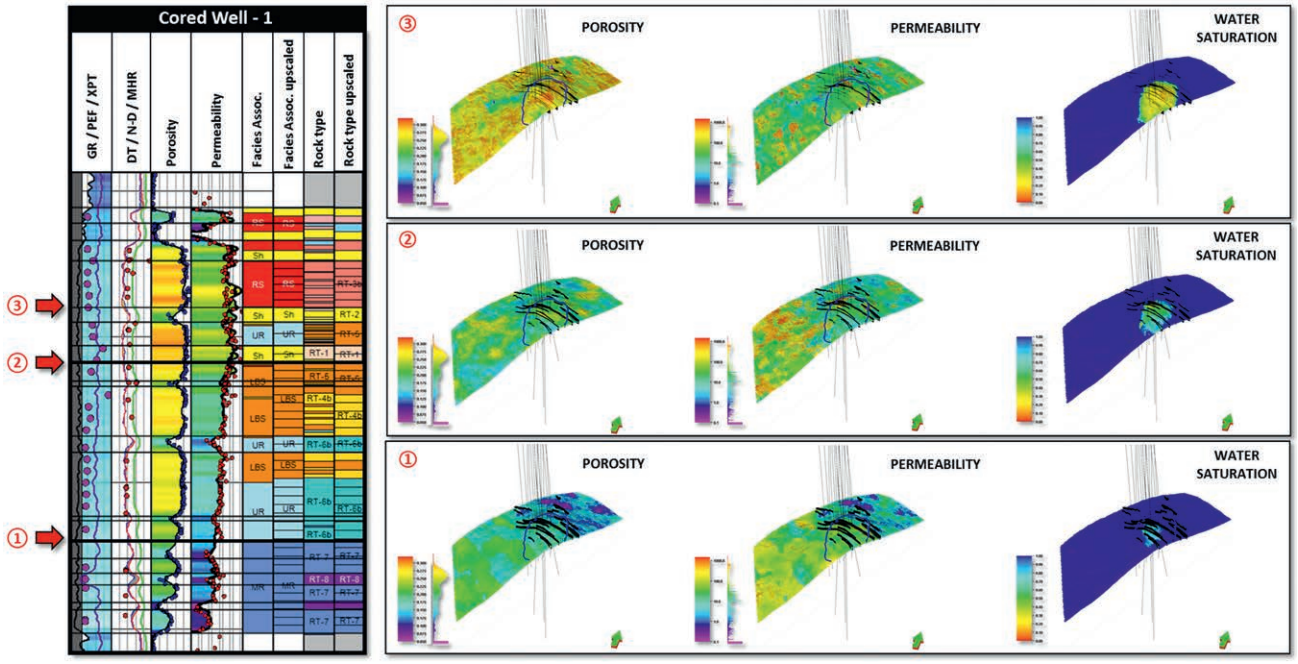

Figure 17 Example of three layers in the geological model illustrating how the property modelling is controlled by the geological model (RRTs) and guided by the porosity cube from the stochastic inversion.

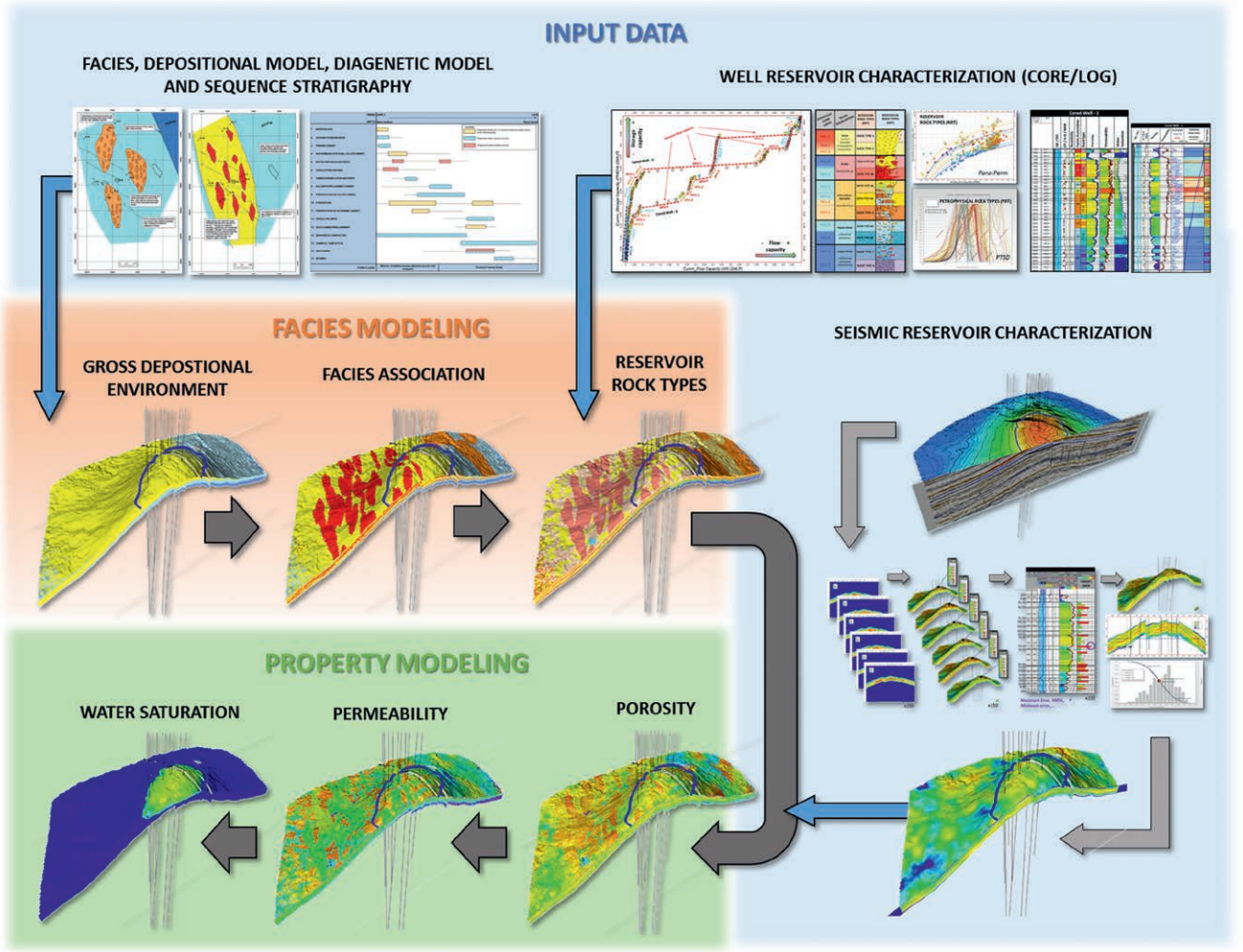

Figure 18 Schematic workflow showing the different steps in the Geological modelling process and how the Sedimentological study and the Seismic Reservoir Characterization Study are integrated in the final 3D Grid.

Property modelling

Property modelling was performed in three main steps: (1) porosity, (2) permeability and (3) water saturation. The distribution of these properties was constrained by the previously modelled RRTs and the interpretation of the free water level (Figure 17).

Porosity input is the well log upscaled to the grid. The porosity is then distributed by a kriging method defining variogram range, nugget, sill and orientation for each RRT. Since well data is sometimes limited, the available deterministic inversion cube was used to extract and compare the horizontal variogram ranges. During the porosity distribution, the selected porosity cube from SI (after screening, Figure 12) was resampled to the geomodel grid. The co-kriging method was used to steer the simulation of the upscaled log porosity by taking the spatial distribution of the porosity cube together with a correlation coefficient (collocated co-kriging). The correlation coefficient between the primary (porosity log upscale) and secondary data (porosity cube SI resampled) can be specified, making it possible to effectively adjust the weight given to the secondary data. The closer the correlation coefficient value is to 1 the higher the weight of the secondary variable (porosity cube). This showed a final porosity realization similar to the results of the SI (i.e. seismically driven porosity). The final goal was to obtain a geomodelled porosity that was driven by the depositional facies model (RRTs) and trended by the seismic information (Figure 15).

The permeability input is the upscaled well log created using the porosity-permeability regression from each RT. To populate the permeability the sequential Gaussian simulation algorithm was used, which is a stochastic method that uses the well data, input distribution variograms and trends to distribute the property through the grid. By changing a seed number, multiple equiprobable realizations were generated to understand the level of uncertainty. The same variograms used in the porosity modelling were used during the simulation. In order to honour the existing relationships between porosity and permeability (per RT), the bivariate transformation (cloud transform) option was used, which includes an input crossplot of primary (permeability) versus secondary data (porosity geomodel). The resulting model honoured the input distribution and followed the same general spatial pattern as the modelled porosity (Figure 16).

Prior to modelling, the cross plot was split into a number of porosity bin intervals. For each porosity bin, a separate distribution and cumulative density function (CDF) was calculated picking randomly a value of permeability to use in the simulation. This crossplot is obtained from the core-data defined for each RT (Figure 16).

Conclusions

This case study highlights the value of an integrated inter-disciplinary study with a common goal of evaluating reservoir quality distribution and providing good-quality input data for geomodelling (Figure 18). An accurate geological model with enhanced predictability capabilities was built, where both fine-scale information provided by wells and sedimentological data could complement seismically-derived attributes in order to distribute final porosity through the reservoir grid.

Acknowledgments

The authors would like to thank ADNOC, ADOC and CGG for permission to publish the results of this study.

References

Buland, A. and Omre, H. [2003]. Bayesian Linearized AVO Inversion. *Geophysics*, **68**(1), 185-198.

Dorn, A.G. [2018]. Structurally Oriented Coherent Noise Filtering. *First Break*, **36**(5), 37-45.

Trudeng, T., Garcia-Teijeiro, X., Rodriguez-Herrera, A. and Khazanehdari, J. [2014]. Using Stochastic Inversion as Input for 3D Geomechanical Models. *International Petroleum Technology Conference*, IPTC 17547.

Strohmenger, C.J. [2006]. High-resolution sequence stratigraphy and reservoir characterization of Upper Thamama (Lower Cretaceous) reservoirs of a giant Abu Dhabi oil field, United Arab Emirates. In: Harris, P.M. and Weber, L.J. (eds.), *Giant hydrocarbon reservoirs of the world: from rocks to reservoir characterisation and modelling.* AAPG Mem. no. 88/SEPM Spec. Publ., 139-171.

Van Buchem, F.S.P. [2002]. Stratigraphic organisation of carbonate ramps and organic-rich intrashelf basins: Natih Formation (middle Cretaceous) of northern Oman. *AAPG Bull*., **86**, 21-53.

Ziegler, M.A [2001]. Late Permian to Holocene Paleofacies Evolution of the Arabian Plate and its Hydrocarbon Occurrences. *GeoArabia*, **6**(3), 445.